Phase Transitions and Conformational Changes in Monolayers of Human Apolipoproteins CI and AII

Jaime Ruiz-García

Instituto de Física, UASLP, Álvaro Obregón 64, San Luis Potosí, S. L. P., México

Abel Moreno

Instituto de Química, UNAM, Circuito Exterior, D. F. 04510, México

Gerald Brezesinski and Helmuth Möhwald

Max-Planck-Institute of Colloids and Interfaces, D-14424 Potsdam, Germany

Jaime Mas-Oliva

Instituto de Fisiología Celular, UNAM, P.O. Box 70-243. D. F. 04510, México

Rolando Castillo*

Instituto de Física, UNAM, P.O. Box 20-364, D. F. 01000, México

Received: March 28, 2003; In Final Form: July 18, 2003

We have studied monolayers of apolipoproteins CI and AII at the air/water interface, observing them along their isothermal compression processes with Brewster angle microscopy and using grazing incidence X-ray diffraction. The lateral order in Langmuir−Blodgett transferred proteins was also studied using atomic force microscopy (AFM). Previous studies have shown that APO CI consists of a chain with two amphiphilic α-helix motifs, whereas APO AII is formed by two identical polypeptide chains, bonded by a disulfide bridge at position 6, where each chain consists also of two amphiphilic α-helix motifs. Monolayers of these proteins exhibit a first-order phase transition between two condensed phases at relatively high values of the lateral pressure and at room temperature. AFM images and X-ray diffraction peaks show that the phase transitions correspond to a phase change from a two-dimensional disordered phase to a more ordered state, where an unusual solid phase is discovered. Here, in each protein chain, one α-helix is confined to the interface, whereas the other α-helix is tilted toward the hydrophobic air.

Introduction

Apolipoproteins (APOs) are a special group of proteins, which are naturally found on the surface of blood circulating lipoprotein particles. Different combinations of lipids, triglyceride derivatives, and proteins produce lipoprotein particles of different density, size, and therefore specific functions related to the metabolism of triglycerides and cholesterol.[1] Two interesting examples of this kind of protein are the exchangeable amphiphilic apolipoprotein CI (APO CI) and apolipoprotein AII (APO AII). APO CI is composed of 57 amino acid residues in length, with a molecular mass of 6.63 kDa. Two crystalline forms of APO CI have been reported as suitable for high-resolution X-ray diffraction analysis.[2] However, its three-dimensional structure still remains unsolved. Secondary structure predictions, nuclear magnetic resonance, and circular dichroism studies made on APO CI have revealed a high α-helix content, distributed in two α-helices.[3−5] The first α-helix (residues 4−30) presents approximately 7.5 periods (a period = 3.6 amino acids of 5.4 Å pitch), while the second one (residues 35−53) consists of 5.2 periods.

APO AII is a protein formed by two identical polypeptide chains bonded by a disulfide bridge at position 6, where each chain corresponds to 77 amino acid residues in length and a molecular mass of 8.708 kDa.[6] Its three-dimensional structure also remains unsolved. Predictive studies have shown that each chain of the APO AII also presents two α-helix motifs (peptides encompassing 7−27 and 32−67) as its main secondary structure.[7] On the basis of its primary structure, all the members of the exchangeable group (CI, AI, AII, CII, CIII, and E) present no similarities among themselves. However, when they are compared at a secondary structure level, important similarities among them appear, mainly due to the presence of amphipathic α-helices.[7−9] The amphiphilic character of both apolipoproteins is based on the fact that a polar protein face is formed due to the clustering of charged amino acid residues on one side, whereas a hydrophobic surface composed of nonpolar residues is formed at the opposite face of the α-helix.[8,9] Hydrophobic moment calculations have confirmed the amphiphilic character of the α-helices in both APOs.[8,9] Since amphiphilicity seems to play a key role in understanding the way these proteins lay down on the surface of lipoprotein particles, the study of amphiphilic apolipoprotein monolayers could provide a model for a better understanding of their physiological behavior. Some apolipoprotein physiological properties are still not well understood, and our results contribute to a better knowledge of the possible conformal changes that might be involved in the process

10.1021/jp034801a CCC: $25.00
Published on Web 09/12/2003

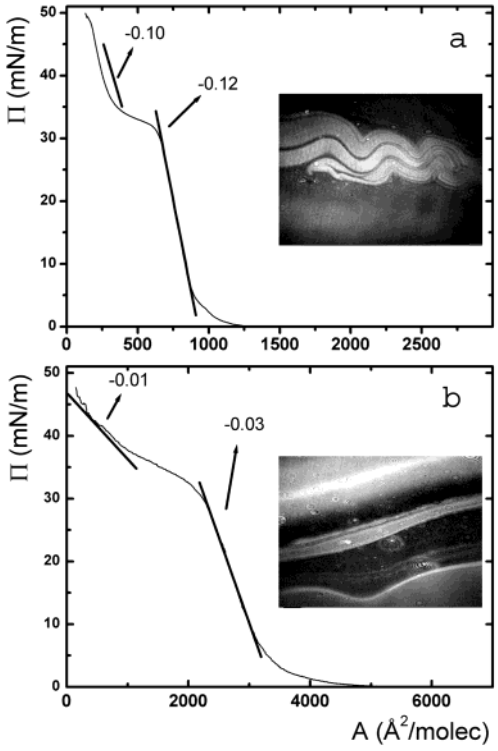

Figure 1. Isotherms Π ($\gamma_o - \gamma$ in mN m^{-1}) vs *A* (area/molecule) for the monolayers of APO CI (a) and APO AII (b) at 25.1 °C.[10] Both proteins were spread onto a subphase of a phosphate-buffered solution (20 mM and pH 8.0) containing 3.5 M KCl. In the insets in both figures, a BAM image of each protein monolayer at the *L*−*LC* coexistence is shown (Π ≈ 33 mN m^{-1} for CI and Π ≈ 35 mN m^{-1} for AII). A feature not captured by the image is that close to the borders of the big bright domains (*LC* phase), it is easy to see streams of the fluid phase *L* (dark area) flowing. Numerical values for the slopes and the lines representing them, above and below the phase transition, are also shown.

of protein exchangeability and lipid exchange between lipoprotein particles and plasma membrane cells.

When APO CI and APO AII are deposited onto a highly ionic water subphase to form a monolayer, two first-order phase transitions are found on compression[8,9] (see Figure 1). The first one involves a condensed fluid phase, which has been denoted as *L*, coexisting with a low-density gaseous phase (*G*), where proteins are weakly interacting, whereas the second one is a transition between two condensed phases: the *L* phase and a new phase denoted by *LC*.[8,9] The transition occurs for APO CI at Π ≈ 33 mN m^{-1} and *A* ≈ 350−600 Å^2 molecule^{-1}, and for APO AII at 30−35 mN m^{-1} and *A* = 1000−2500 Å^2 molecule^{-1}.[10] A model for both proteins at the air−water interface has been suggested. APO CI is modeled as two amphiphilic α-helices of approximately 28.5 and 40.5 Å in length, bonded by a loose hinge,[8] and APO AII as two amphiphilic chains bonded at position 6, where each chain has two α-helices, also bonded by a loose hinge, of approximately 31.5 and 54 Å in length.[9] The second phase transition in both proteins has been suggested to be due to a conformational change, where one α-helix segment as in the case of APO CI[9] or two α-helix segments as in the case of APO AII[8] desorb from the subphase. However, no direct evidence of this conformational change has been shown.

Although the most common way for studying monolayers is the measurement of surface pressure/area isotherms and observing them during the process of compression with Brewster angle microscopy (BAM), the use of grazing incidence X-ray diffraction (GIXD)[11] can yield information about the molecular organization of ordered phases present in the monolayer. A wealth of mesophases has been detected using this technique.[12] In this study, we investigated the organization of the condensed phases present in the monolayers of both apolipoproteins APO CI and APO AII, using GIXD experiments. Lateral order in Langmuir−Blodgett films of transferred monolayers for both proteins was also studied with atomic force microscopy (AFM). We show direct evidence that at the *L*−*LC* phase transition both apolipoprotein monolayers go from a two-dimensional disordered to an ordered state, where one of the α-helix segments in each polypeptide chain is confined to the interface, whereas the other α-helix segment in the chain is desorbed from the water subphase and tilted toward the hydrophobic air.

Experimental Section

Apolipoproteins and Subphase. Lyophilized human APO CI (98%, PerImmune Inc., MD) and APO AII (>95%, Calbiochem, CN Biosciences, CA) were solubilized in a buffered solution (pH 8.0) and filtered with a 0.22 μm membrane filter, prior to being spread onto a subphase made of a phosphate-buffered solution of 3.5 M KCl (Baker, Mexico) prepared with ultrapure water (Nanopure-UV, 18.3 MΩ cm resistivity).[8,9] The subphase buffered solution was prepared with sodium phosphate at a concentration of 20 mM and pH 8.0. It is important to note that before preparing these solutions the KCl salt was heated for 4 h at 300 °C to prevent, when dissolved, traces of organic compounds in the subphase.[8,9]

Langmuir and Langmuir−Blodgett Films. Apolipoprotein monolayer isotherms and transferred LB films were prepared on a computerized Nima LB trough (TKB 2410A, Nima Technology Ltd., England) using a Wilhelmy plate to measure the lateral pressure, Π = $\gamma_o - \gamma$, i.e., the surface tension difference of the clean subphase and that of the protein-covered subphase. Temperature was kept constant at 25 °C with the aid of a water circulator bath (Cole-Parmer 1268-24). The speed of compression was around 50 cm^2/min. All experiments were carried out in a dust-free environment. All monolayers used to obtain isotherms and LB film were observed with a BAM1 Plus (Nanofilm Technologie GmbH, Germany) Brewster angle microscope. We transferred APO CI and APO AII on mica, cleaved just before the deposition at a speed of ∼2 mm min^{-1}. The lateral pressure for transferring the monolayer in the *LC* phase was fixed ca. 43 mN/m for APO CI and ca. 38 mN/m for APO AII. The AFM scanning was performed just after LB preparation.

GIXD Experiments. Synchrotron X-ray experiments carried out on APO CI and APO AII monolayers were performed at the beam line BW1 at Hasylab, DESY (Hamburg, Germany). The grazing incidence angle α_i of the monochromated X-ray beam (λ = 1.304 Å) was adjusted to be approximately equal to 0.85α_c, where α_c is the critical angle for total reflection, which maximizes the surface sensitivity and reduces the background scattering from the subface. The dimensions of the X-ray beam footprint on the interface were ∼2 × 50 mm^2. GIXD diffraction peaks were obtained from ordered domains, which have a random orientation in the water plane. The scattered intensity was detected by a position-sensitive detector (PSD) along the vertical component of the X-ray scattering vector, $q_z = (2\pi/\lambda)$ sin α_f, where α_f is the angle between the horizontal plane and the diffracted beam. Measurements were performed by scanning over a range along the horizontal scattering vector, $q_{xy} = (4\pi/\lambda)$ sin θ_{xy}, where $2\theta_{xy}$ is the angle between the incident and diffracted beams projected onto the horizontal plane. Thus, the scattering vector is $\boldsymbol{q} = \boldsymbol{q}_{xy} + \boldsymbol{q}_z$. Our diffraction data are

TABLE 1: X-ray Parameters of Monolayers of APO CI and APO AII[a]

protein	q_{xy}, Å^{-1}	q_z, Å^{-1}	Δq_{xy}, Å^{-1}	Δq_z, Å^{-1}	d, Å	ξ_{xy}, Å	h, Å
			Below Transition				
APO CI			no diffraction peaks were observed				
APO AII	0.577 ± 0.002	0.005 ± 0.001	0.136	1.199	10.9	41	5.2
			Above Transition				
APO CI (expt 1)	0.516 ± 0.001	0.338 ± 0.002	0.0252	0.357	12.2	220	15.5
APO CI (expt 2)	0.514 ± 0.001	0.317 ± 0.002	0.0353	0.348	12.2	158	15.9
APO AII (peak 1)	0.509 ± 0.001	0.320 ± 0.002	0.0429	0.304	12.3	129	18.19
APO AII (peak 2)	0.251 ± 0.001	0 ± 0.001	0.0385	0.437	25.1	144	12.6

[a] q_{xy} is the Bragg peak position. q_z is the Bragg rod position. Δq_{xy} is the fwhm of the Bragg peak. Δq_z is the fwhm of the Bragg rod. d is the repeating distance. ξ_{xy} is the in-plane correlation length. h is an estimate of the thickness.

represented in two ways: (a) using the GIXD pattern $I(q_{xy})$ obtained by integrating over the whole q_z window of the PSD showing the Bragg peaks and (b) using the Bragg rod intensity profiles, which are the scattered intensity $I(q_z)$ recorded in channels along the PSD but integrated over the q_{xy} range of each Bragg peak. Different kinds of information may be extracted from the measured profiles. The $2\theta_{xy}$ (or q_{xy}) positions of the Bragg peaks yield the lattice repeat distances $d = 2\pi/q_{xy}$, which can be indexed by two Miller indices (h,k) to yield the unit cell. The full-width at half-maximum (fwhm) of the Bragg peaks (Δq_{xy}) corrected by instrumental resolution (0.008 Å) yields an estimate of the in-plane coherence length, $\xi_{xy} \approx 0.88 \times 2\pi/(\Delta q_{xy})$. The fwhm of the Bragg rod intensity profile gives an estimate of the film thickness $h_z \approx 0.88 \times 2\pi/(\Delta q_z)$.

AFM Observations. Transferred monolayers of both APOs were scanned with a NanoScope IIIa SPM (Digital Instruments, CA) with a 15×15 μm scanner. Preliminary scanning runs were made to define the specific area to be studied. Depending on the case, we used contact, intermittent contact, and deflection modes to obtain topographic and deflection images at different frequencies, using Si_3N_4 tips with a typical force constant of 0.3 Nm^{-1}. We employed a low scan rate of 1 Hz, and the images were analyzed using the Digital Instruments software. Scans for 30−50 Hz were also performed to detect noise artifacts, and the scan angle was changed several times in different directions to discern between real images of the protein films from those corresponding to noise. It is worth mentioning that lipoprotein LB films transferred onto mica presented small KCl crystals along their surface, crystallized from the subphase during deposition. AFM images were obtained at low magnification, and once a proper flat area without salt crystals was found, the scanning was changed to a higher resolution. Extreme care was needed to avoid KCl crystals in the area under study to prevent tip damage and noise artifacts. Height images were normally noisy, whereas deflection images were usually good enough. Therefore, the AFM images presented here are deflection images unless indicated otherwise.

Results and Discussion

In Figure 1, we present typical isotherms for the monolayers of APO CI and APO AII at the air/water interface (highly ionic). BAM images show a $L-LC$ first-order phase transition for both proteins at relatively high lateral pressure where isotherms show a change in slope. Here, bright domains of LC phase are in coexistence with a dark disordered phase L. The bright domains are nucleated from the L phase. A detailed discussion of the features of these isotherms can be found elsewhere.[8,9]

To obtain insight into the molecular order in the L and LC phases, GIXD experiments were performed for both proteins (results are presented in Table 1) below and above the phase transition of interest here. Below the phase transition, no diffraction peaks were detected for APO C1, confirming the 2D liquidlike nature proposed for this phase.[9] However, for the APO AII we observed a very broad peak (see Figure 2) corresponding to an average repeating distance of 10.9 Å, with an in-plane correlation length of $\xi_{xy} = 41$ Å. Since APO AII is formed by two relatively rigid chains, and each chain is composed of two α-helices, the repeating distance should be the average interaxis separation between these two chains, which are bonded at position 6. In addition, the in-plane correlation length is quite short; it is on the order of about 4 times the repeating distance. Thus, we assigned a 2D liquidlike order to this phase.

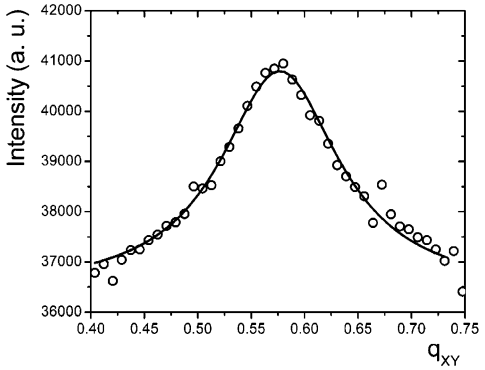

Figure 2. Bragg peak obtained for the APO AII monolayer in the L phase. X-ray scattering intensity as a function of the in-plane component of the momentum transfer vector q_{xy} (Å^{-1}).

Above the phase transition, only one diffraction peak was detected for APO CI, corresponding to a repeating distance of 12.2 Å, as shown in Figure 3a. Our calculated value for the in-plane correlation length is $\xi_{xy} = 160-220$ Å. The position of the Bragg rod presented in Figure 3b is located at a nonzero q_z value. Therefore, the ordered phase is most certainly composed of tilted helices[12] with an unknown tilt direction, since it cannot be determined from a sole nonzero q_z diffraction peak. An out-of-plane coherent height of 15.5 Å was calculated for the ordered phase by fitting a Gaussian profile to the Bragg rod peak. The coherent height is about half the length of the smaller α-helix, probably indicating that the tilted α-helices are not completely ordered along their full length. We want to point out that, since there is only one diffraction peak, the order extends in one direction only. This kind of order is unexpected, because to our knowledge, no quasi-one-dimensional order has been found in organic molecules or biomacromolecules. Nevertheless, there are a few examples of this kind of order in inorganic compounds.[13]

For the case of APO AII, we obtained two diffraction peaks for a pressure above the phase transition, as shown in Figure 4 and Figure 5. In Figure 4, the repeating distance is 12.3 Å, quite similar to the repeating distance found for APO CI. Here, the

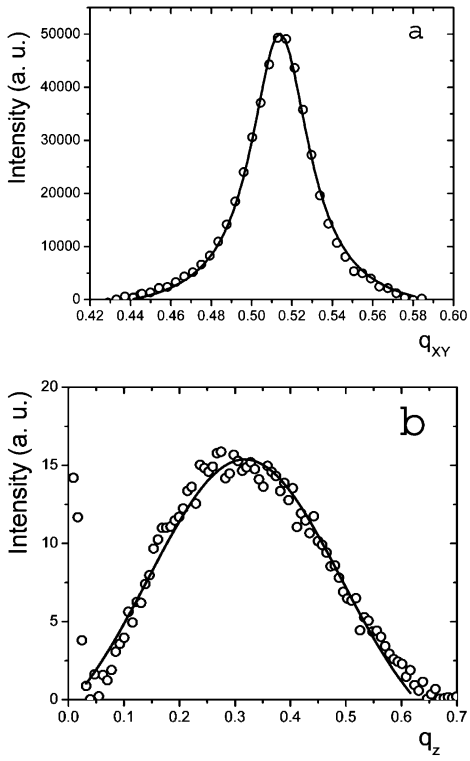

Figure 3. GIXD measurements for the APO CI monolayer in the *LC* phase. (a) Bragg peak: X-ray scattering intensity as a function of the in-plane component of the momentum transfer vector q_{xy} (Å^{-1}). (b) Bragg rod: X-ray scattering intensity as a function of the vertical component of the momentum transfer vector q_z (Å^{-1}).

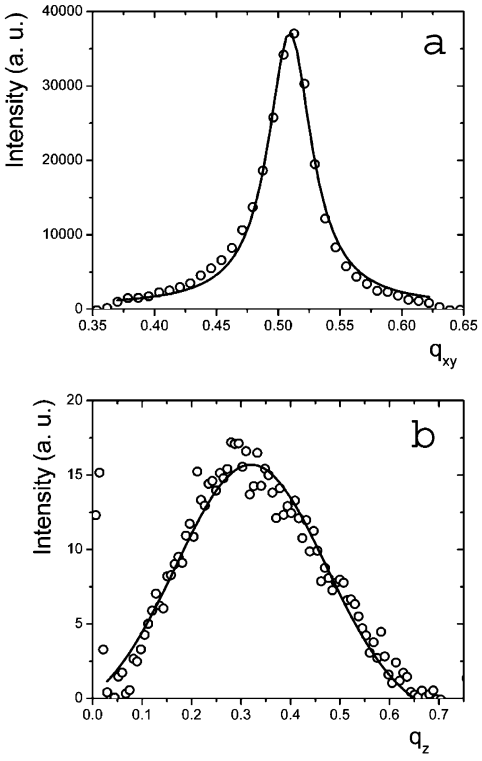

Figure 4. GIXD measurements for a first peak of the APO AII monolayer in the LC phase. (a) Bragg peak: X-ray scattering intensity as a function of the in-plane component of the momentum transfer vector q_{xy} (Å^{-1}). (b) Rod peak: X-ray scattering intensity as a function of the vertical component of the momentum transfer vector q_z (Å^{-1}).

in-plane correlation length, ξ_{xy}, is 130 Å. The position of the Bragg rod is also located at a nonzero q_z value. The second

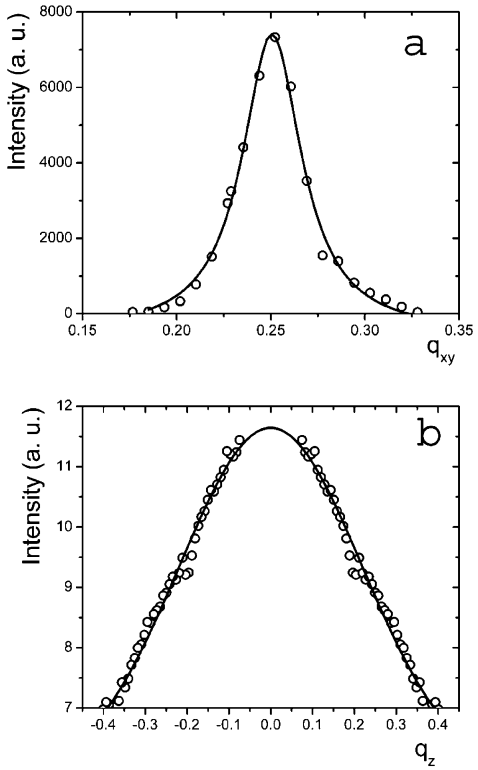

Figure 5. GIXD measurements for a second peak of the APO AII monolayer in the *LC* phase. (a) Bragg peak: X-ray scattering intensity as a function of the in-plane component of the momentum transfer vector q_{xy} (Å^{-1}). (b) Rod peak: X-ray scattering intensity as a function of the vertical component of the momentum transfer vector q_z (Å^{-1}). The negative branch was obtained by reflection of the positive branch to obtain a good Gaussian fitting.

peak (see Figure 5) at $q_z \approx 0$ has a repeating distance of 25.1 Å, with an in-plane correlation length of ∼144 Å. The out-of-plane coherent height for this case is 18.2 Å, calculated by fitting a Gaussian profile to the Bragg rod peak. Similar to the case of APO CI, the coherent height is also less than the length of any of the α-helices, probably indicating here, as well as there, that the tilted α-helices are not completely ordered along their full length. Although, if one determines a rectangular unit cell from the two peaks found for APO AII, the short side of the rectangle would be 12.74 Å and the long one 50.06 Å. Since such a unit cell is not consistent with the AFM data of molecular models, we think that the two repeating distances are independent of each other.

Langmuir−Blodgett films of APO CI and APO AII were transferred on mica and surveyed with AFM to get an independent picture of lateral order of the monolayers. Conformation of proteins whether in solution or adsorbed onto a solid substrate is determined by a delicate balance of intramolecular and intermolecular interactions. Nevertheless, although structure modification caused by the transfer and subsequent adsorption of the helices is expected, these changes are not relevant in condensed phases transferred at low rates.[14,15]

Figure 6 shows an AFM image for a transferred monolayer of APO CI in the *L* phase. This image shows semiordered stripes whose width ranges from 0.4 to 0.9 nm. The width of the stripes corresponds approximately to the width of a single protein chain. The length of the stripes cannot be clearly determined because they are not completely continuous and straight. Nevertheless, one can find along the images some stripes with a length close to the value of the whole Apo CI (∼8.5 nm) or of their α-helices (4.0 and 2.8 nm). Taking into account that the stripes change

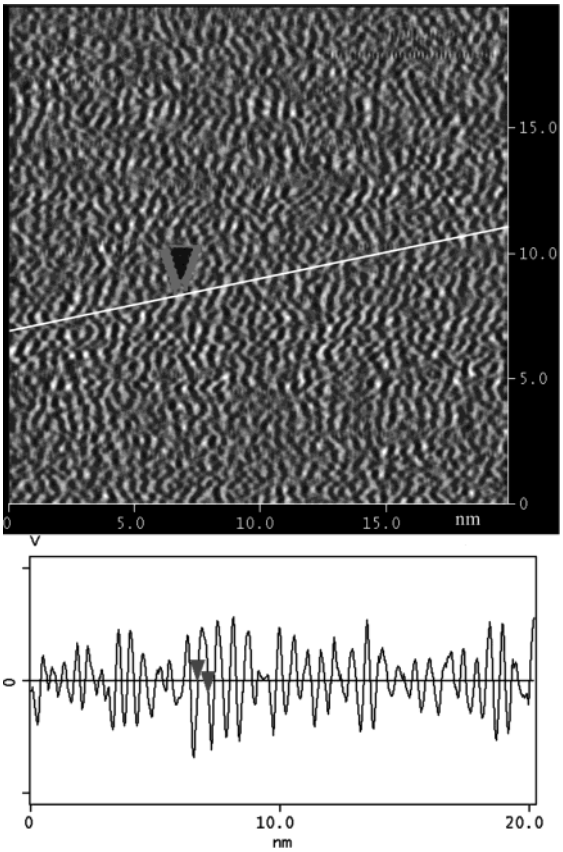

Figure 6. AFM image of a monolayer of Apo CI transferred on mica at 25 °C and $\Pi = 20$ mN m^{-1} (below the phase transition) and its vertical voltage profile. The horizontal distance between the arrows in this case is 0.5 nm, which is of the order of the α-helix diameter.

their alignment direction continuously along areas larger than those shown in Figure 6, the positional order seems to be short-ranged. Thus, the lack of long-range order of the transferred monolayers, the fluidity observed with BAM, and the lack of X-ray diffraction peaks, as shown above, seem to confirm the 2D liquidlike nature proposed for the *L* phase.[9]

In Figure 7, we present a typical height AFM image of the *L* phase monolayer of Apo AII transferred on mica. The main feature observed here is that Apo AII self-organizes in bright rows lying down on a flat dark surface (mica). The bright row width in Figure 7 is ca. 1.7 nm, although we observed that these rows could reach a width up to 2.0 nm in different transferred monolayers. This width corresponds nearly to double the value of the APO AII dimeric protein. This result is quite suggestive, because if the bright row width corresponds to surveying a dimer perpendicularly with the AFM tip, then this width must be the sum of the interaxis separation between the two chains measured by GIXD (10.9 Å) plus two times the α-helix radius (∼5 Å) corresponding to the two chains forming the dimer; this adds up to ∼16 Å, which is in excellent agreement. Thus, the AFM images for the *L* phase of the APO AII monolayer transferred on hydrophilic mica strongly suggest that the rows are formed by the APO AII dimers, where both polypeptide chains are lined up, more or less parallel to each other, lying down on the water surface, with the hydrophobic face exposed to the air; this agrees with the structure of APO AII given above. The order in the *L* phase of the APO AII monolayer seems to be larger than in the case of the *L* phase of the APO CI monolayer, probably due to the presence of the disulfide bridge.

Figure 8 shows a typical AFM image of a transferred monolayer of APO CI above the phase transition (*LC* phase)

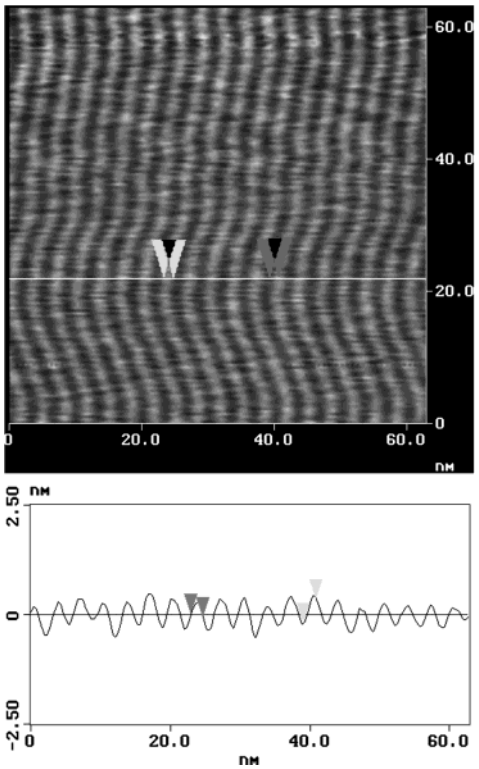

Figure 7. AFM height image of the *L* phase of the Apo AII monolayer transferred on hydrophilic mica (∼20 mN m^{-1}) at 25 °C and a vertical cross section along the line crossing the image. The length between the dark arrows is 1.7 nm, and the height between the gray arrows is 0.54 nm.

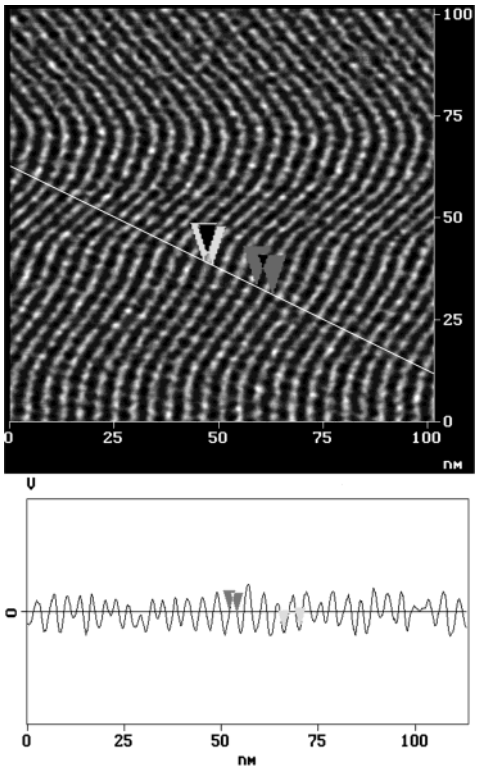

Figure 8. AFM image of a transferred monolayer of APO CI on mica at $\Pi = 43$ mN m^{-1} (above the *L*−*LC* phase transition). Vertical voltage profile: horizontal distance between gray arrows 2.0 nm; horizontal distance between black arrows 4.2 nm.

on hydrophilic mica and a vertical profile. Here, we observe bright rows separated by dark rows, which are located at different levels as shown by their different brightness. The bright

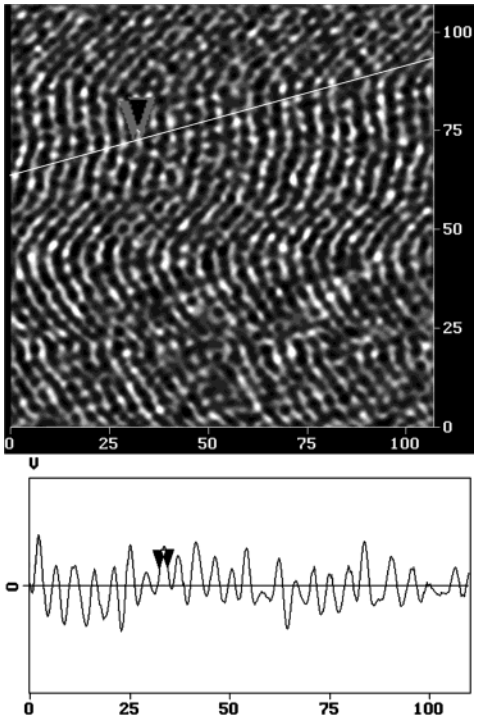

Figure 9. AFM image of the APO AII monolayer in the *LC* phase transferred on hydrophilic mica at *25* °C and a vertical voltage cross section along a line crossing the image. The length between the arrows is 2.1 nm.

rows present a width between 15 and 20 Å. A vertical profile along these bright rows reveals a profile with peaks that are not regularly disposed, not allowing a meaningful distance along the top of the rows to be obtained. This probably is in agreement with the coherence height, which indicates that the tilted helices are not well ordered along their full length. The average center-to-center distance between the black rows is 41.1 ± 2.8 Å. The dark rows do not correspond to bare mica. Vertical profiles show bumps perpendicular to the row axis of a width close to the diameter of an α-helix. Although these measurements are quite noisy, it is clear that the mean distance between the bumps is 11.7 ± 2.6 Å (not shown in Figure 8).

Figure 9 shows an AFM image of a monolayer of APO AII in the *LC* phase transferred ($\Pi \approx 38$ mN/m) on mica. It clearly shows the formation of bright and dark rows, indicating different heights. The height along the top of the bright rows is not uniform probably due to the coherence height, which indicates that the tilted helices are not well ordered along their full length. The bright rows have a width of ca. 20 Å. The average center-to-center distance between the dark rows is 35.2 ± 4 Å. The formation of these bright rows seems to be similar to the case of APO CI, where a part of the protein molecule desorbs from the water surface and another remains grafted to the surface. In this case, probably two α-helices of the protein molecule desorb from the surface, since APO AII has two identical amphiphilic polypeptide chains, each one with two α-helices, bonded by poorly structured polypeptide fragments. This conformational change, where two α-helices are desorbed from the water/air interface leaving the other pair of α-helices on the surface, explains the large area per molecule change along the *L*−*LC* phase transition in the isotherm.[8] This also agrees with the images obtained with BAM,[8] a technique sensitive to differences in thickness of monolayers, along the *L*−*LC* phase transition. Here, the different levels of reflectivity between the *LC* domains (higher) and the *L* domains (lower) reveal different monolayer

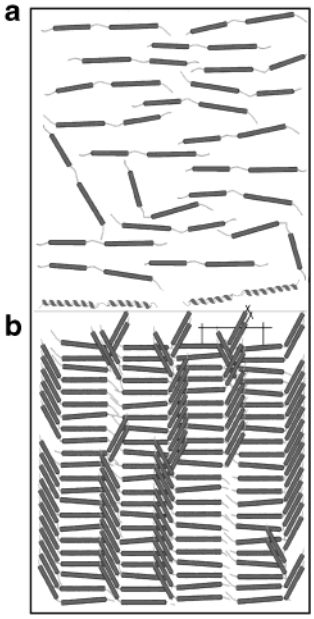

Figure 10. Model for the APO CI monolayer at the air/water interface: (a) below and (b) above the *L*−*LC* phase transition.

thickness. The question of what pair of α-helices is desorbed from the water surface, those encompassing residues 7−27 or those encompassing residues 32−67, can be solved considering the hydrophobic moments. There is a high probability that the smaller α-helices, which have a higher hydrophobic moment ($\mu H = 0.49$ kcal/mol) than the larger ones ($\mu H = 0.34$ kcal/mol),[8] remain on the water surface. AFM seems to confirm this fact, since AFM images for the *LC* phase show an average separation distance of 35.2 Å between dark rows, which is a distance similar to the length of the smaller α-helices (∼31.5 Å) and much shorter than the length of the large α-helices (∼54 Å).

All experiments presented above enabled us to propose a model for both apolipoproteins studied here. In both cases, we have a disordered 2D liquid in the *L* phase, as shown in Figures 10a and 11a. In this liquid, the proteins are traveling in a landscape of close energy minimum configurations, where the different protein configurations have the restriction of lying down along the long axis of the α-helices on the subphase. Here, the hydrophilic faces of the α-helices are in contact with the water subphase and the hydrophobic faces are oriented toward the air. One important point to be mentioned here is that we have obtained the average distance between the bonded polypeptide chains for the APO AII (10.9 Å).

Above the phase transition pressure, in the *LC* phase, an α-helix segment of each polypeptide chain is desorbed from the water surface. Figures 10b and 11b present our proposed molecular arrangement model for the *LC* phase of both proteins. In APO CI, the X-ray repeating distance of 12.2 Å and the nonzero Bragg rod arise from the desorbed α-helices with an in-plane correlation involving about 13−18 α-helices. The α-helices lying down seem to be the long ones, in agreement with the center-to-center distance between rows measured by AFM (41.1 Å). AFM images of this phase show a remarkable arrangement of rows formed by walls generated by the desorbed α-helices. However, a question arises: Why don't these apparent well-ordered walls give rise to a diffraction peak with a repeating distance similar to that found in the AFM image? The answer is probably as follows: The repeating distance from the AFM image is 41.1 Å; thus, one should expect a diffraction peak to appear at $2\theta \approx 1.8$. This is an angle quite close to the direct

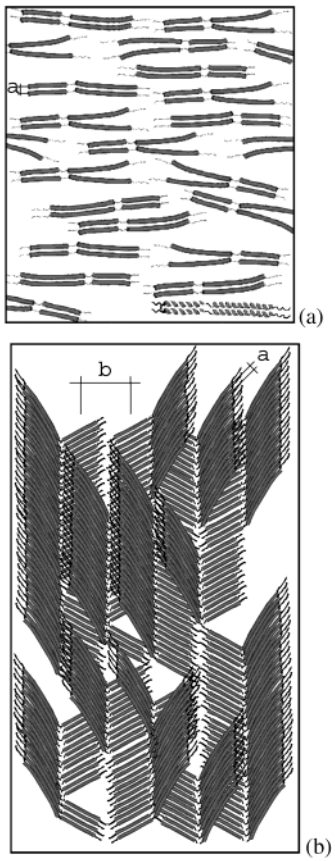

Figure 11. Model for the APO AII monolayer at the air/water interface: (a) below the *L*−*LC* phase transition and (b) above *L*−*LC* phase transition.

beam, but still experimentally accessible. We performed careful experiments around this angle, and no diffraction peak was found. A plausible explanation for the lack of this peak is that the correlation between the walls formed by the desorbed α-helices is short-ranged; that is, the correlation among walls has a liquidlike order. This is possible because this phase nucleates from an isotropic phase, and many defects prevent annealing due to the geometry of the proteins and to the 2D confinement. At the phase transition, when the smaller α-helices desorb from the surface, the walls are not in perfect registry with each other, since the tilt direction of the α-helices forming the walls (bright rows) can be randomly distributed to the left or the right of a symmetry plane perpendicular to the water surface; see Figure 10b. The random orientation of the desorbed α-helix tilt angle probably introduces enough disorder to prevent a quasi-long-range order and, as a consequence, the lack of a diffraction peak.

In APO AII, we have two X-ray repeating distances, 12.3 and 25.1 Å. The first repeating distance is quite similar to the APO CI repeating distance for the desorbed α-helices. Therefore, it should come from the ordering of desorbed α-helices and has a correlation involving, on the average, 10 α-helices. The second repeating distance corresponding to the peak at $q_z \approx 0$ is close to the center-to-center distance between black rows observed in the AFM images (35.2 Å) and probably corresponds to the stripes formed by the α-helices lying down in Figure 11b. The α-helices lying down seem to be the shorter ones, as mentioned above. The disulfide bridge present at position 6 constrains the degrees of freedom of the polypeptide chains, so it could explain the high order probed by the GIXD experiments, giving rise to the diffraction peak at $q_z \approx 0$. The walls generated by the desorbed α-helices are tilted to different sides, preventing the appearance of any X-ray scattering peak, as in the case of APO CI. Therefore, we modeled the molecular arrangement of the *LC* phase of APO AII like ordered walls of tilted α-helices separated by rows of α-helices parallel to the water surface, as shown in Figure 11b. No correlation is proposed among the walls of tilted helices; therefore, they can also be regarded as a quasi-one-dimensional solid.

In general, one would expect that the slope of an isotherm, which is directly related to the compressibility coefficient, of a well-ordered phase should be higher than the slope of a disordered phase. In the case of APO AII, we found that the slope of the *LC* phase isotherm is 3 times smaller than that of the *L* phase (see Figure 1). When the longer α-helices desorb from the surface, they leave room that cannot be easily covered by the smaller α-helices, making this phase highly compressible. This fact could also explain the difference between the center-to-center distance measured between the dark rows (35.2 Å) in the AFM images and the GIXD repeating distance (25.1 Å). These distances must be very sensitive to the lateral pressure where the measurements are performed. In contrast, *L* and *LC* phases of APO CI show the same isotherm slopes, indicating that when the smaller α-helices desorb, the longer-ones grafted to the surface rearrange themselves in the room left by the desorbed helices, leading to interactions among the polypeptide chains quite similar to those in the *L* phase.

Conclusions

The air/water interface offers a good media to study protein films in a controlled way, at a well-defined temperature, lateral pressure, film, and subphase composition. Here, we have shown how proteins with high α-helix content, such as APO CI and Apo AII, can form Langmuir monolayers at the air/water interface (highly ionic). Upon compression, both protein monolayers self-assemble into a dense two-dimensional liquidlike phase that undergoes a conformational phase transition at relatively high lateral pressure. For APO CI this conformational phase transition is observed at 33 mN/m. GIXD results confirmed that the phase below the transition pressure presents a 2D liquid structure. We modeled this phase as an ensemble of two α-helices bonded with nonstructured peptides acting as a hinge and lying down randomly on the water surface. Unexpectedly, the phase above the transition pressure showed only one diffraction peak, indicating that the order goes only in one direction. For the dimeric APO AII, the transition occurs at about 30−35 mN m^{-1}. The phase below the transition pressure showed a liquidlike structure, although it showed a broad diffraction peak. However, it corresponds to the interaxis separation between the sulfur-bonded chains. The phase above the transition pressure showed also an arrangement of rows of tilted helices and helices parallel to the surface. This arrangement exhibits two diffraction peaks: one is associated with the tilted helices order and the other is associated with the order between rows formed by the helices lying down on the surface. The two diffraction peaks seem to be uncorrelated to each other.

Our results suggest that at particular lateral pressures, i.e., when the *L*−*LC* phase transitions occur, conformational changes take place in these monolayers. Therefore, we might put forward the possibility that similar conformational changes could also be occurring in both proteins in response to changes in surface pressure, when located at the surface of lipoprotein particles. If we visualize these conformational changes, for instance, as part of a triggering mechanism sensitive to changes in lateral pressure, secondary to changes in size and composition of

lipoproteins, we believe that the observations made in this study could have new and important implications in the complex mechanisms involved in the exchange of apolipoproteins between lipoprotein particles and in the way lipid is transferred between lipoproteins.

Acknowledgment. We acknowledge the financial support provided by CONACYT, DGPA-UNAM (R.C. and J.M-O.), SEP, and The Alexander von Humboldt Foundation (J.R.-G.). We also thank HASYLAB at DESY (Hamburg, Germany) for the beam time, and S. Ramos, J. Xicohtencatl-Cortes, and C. Garza for their technical assistance.

Note Added after Print Publication. A transcription error resulted in an erroneous Figure 8 when this Article was published on the Web 9/12/2003 (ASAP) and in the October 9 issue (Vol. 107, No. 40, p 11121). The electronic version of the Article was corrected on 10/24/2003 and an Addition and Correction appears in the November 20, 2003, issue (Vol. 107, No. 46).

References and Notes

(1) Voet, D.; Voet, J. G. *Biochemistry*, 2nd ed.; John Wiley: New York, 1995; p 314.

(2) Weisgraber, K. H.; Newhouse, Y. M.; McPherson, A. *J. Mol. Biol.* **1994**, *236*, 382.

(3) Rozek, A.; Buchko G. W.; Kanda, P.; Cushley, R. J. *Protein Sci.* **1997**, *6*, 1858.

(4) Rozek, A.; Buchko, G. W.; Cushley, R. J. *Biochemistry* **1995**, *34*, 7401−7408.

(5) Buchko, G. W.; Rozek, A.; Zhong, Q.; Cushley, R. J. *Peptide Res.* **1995**, *8*, 86.

(6) Brewer, H. B.; Lux, S. E.; R. Ronan, John, K. M. *Proc. Natl. Acad. Sci. U.S.A.* **1972**, *69*, 1304.

(7) Bolaños-Garcia, V. M.; Soriano-Garcia, M.; Mas-Oliva, J. *Mol. Cell. Biochem.* **1997**, *175*, 1.

(8) Bolaños-Garcia, V. M.; Ramos, S.; Castillo, R.; Xicohtencatl-Cortes J.; Mas-Oliva, J. *J. Phys. Chem. B* **2001**, *105*, 5757.

(9) Bolaños-Garcia, V. M.; Mas-Oliva, J.; Ramos, S.; Castillo, R. *J. Phys. Chem. B* **1999**, *103*, 6236.

(10) Improved isotherms for APO CI were obtained here with new samples of this protein, which are of higher quality than those used in ref 9. Data for Apo AII come from ref 8.

(11) Als-Nielsen, J.; Jacquemain, D.; Kjaer, K.; Leveiller, F.; Lahav, M.; Leiserowitz, L. *Phys. Rep.* **1994**, *246*, 251.

(12) Kaganer, V. M.; Möhwald, H.; Dutta, P. *Rev. Mod. Phys.* **1999**, *71*, 779.

(13) Andreas, E.; Müller, D. J. *Nat. Struct. Biol.* **2000**, *7*, 715.

(14) Burkett, S. L.; Read, M. J. *Langmuir* **2001**, *17*, 5059.

(15) Leporatti, S.; Brezesinski, G.; Möhwald, H. *Colloids Surf. A* **2000**, *161*, 159.